# Effects of electrode-molecule binding and junction geometry on the single-molecule conductance of bis-2,2′:6′,2″-terpyridine based complexes

Ross Davidson,[a] Oday A. Al-Owaedi,[b,c] David C. Milan,[d] Qiang Zeng,[e,f] Joanne Tory,[e] František Hartl,[e]* Simon J. Higgins,[d] Richard J. Nichols,[d]* Colin J. Lambert,[b]* Paul J. Low[g]*

[a] Department of Chemistry, Durham University, South Rd, Durham, DH1 3LE, UK.

[b] Department of Physics, Lancaster University, Lancaster, LA1 4YB, UK.

[c] Department of Laser Physics, Women Faculty of Science, Babylon University, Iraq.

[d] Department of Chemistry, University of Liverpool, Crown St, Liverpool, L69 7ZD, UK.

[e] Department of Chemistry, University of Reading, Whiteknights, Reading, RG6 6AD, UK.

[f] School of Chemistry and Chemical Engineering, South China University of Technology, Guangzhou, 510640, PR China.

[g] School of Chemistry and Biochemistry, University of Western Australia, 35 Stirling Highway, Crawley, Perth, WA 6009, Australia.

*Email: f.hartl@reading.ac.uk, r.j.nichols@liverpool.ac.uk, c.lambert@lancaster.ac.uk, paul.low@uwa.edu.au*

**ABSTRACT:** The single molecule conductances of a series of bis-2,2′:6′,2″-terpyridine complexes featuring Ru(II), Fe(II) and Co(II) metal ions and trimethylsilylethynyl ($Me_3SiC{\equiv}C$-) or thiomethyl (SMe) surface contact groups have been determined. In the absence of electrochemical gating, these complexes behave as tunneling barriers, with conductance properties determined more by the strength of the electrode-molecule contact and the structure of the 'linker' than the nature of the metal-ion or redox properties of the complex.

## INTRODUCTION

The development of methods that permit the measurement of the electrical characteristics of single molecules under routine laboratory conditions,[1,2] coupled with the incentives for technological innovation arising from ever increasing challenges facing top-down miniaturisation of solid-state electronic devices, has seen a renaissance in the field of molecule electronics over the past decade.[3-6] In the context of developing molecular components for use in a hybrid solid-state / molecular electronics technology, many different molecular structures have been examined within molecular junctions, including oligophenylenes,[7] oligoaryleneethynylenes,[8] and oligoynes,[9] and arylene–ethynylene based molecular wires up to 8 nm in length.[10-12] However, whilst the majority of metal|molecule|metal junctions studied to date has been derived from organic molecules, the possibility that metal complexes may play a role in molecular electronics has been recognized,[13] and inorganic and organometallic molecular components for electronics are now attracting increasing attention.[14-18]

Various families of metal complexes have been explored for their wire-like properties and higher functionalities,[19,20] including porphyrin oligomers[21] and

assemblies[22] and metal alkynyl complexes.[23-28] Within the context of exploratory studies, bis-2,2′:6′,2″-terpyridine complexes are particularly attractive, being compatible with a broad cross-section of the metallic elements of the transition series, and thereby offering a wide range of metal d-electron configurations and charges, electro- and photo-chemical activity, and diverse synthetic approaches which include 'on surface' strategies that been used in the construction of quite complex surface bound mono-[29] and multi-metallic[30-32] films with impressive electrical characteristics.[33-38] Within single molecule junctions, the flexibility of the coordination bonds around the metal center has led to the opportunity for manipulation of transport properties through such 'Cardan-joint' style metal complexes by mechanical stimulus.[39,40]

Regardless of the method of assembly, as components in molecular electronics, metal complexes offer the potential for finer tuning of the frontier molecular orbitals in metal complexes to match the Fermi levels of the electrodes,[41] the possibilities of augmenting electronic characteristics through accessing available redox levels[42] and manipulating them through electrochemical gating,[43-45] the introduction of magnetic effects,[46,47] and high thermoelectric efficiency.[48] These various factors are then expanded further by experimental and computational work in which multiple metal centers are introduced along a linear 'wire-like' chain, either as an array of metal atoms[14,49,50] or in ligand-linked assemblies.[24-27]

Whilst there is a body of experimental evidence, such as the observation of Kondo effects in transition metal complex based molecular junctions[51-53] and electrostatically gated spin-blockade effects,[46] which indicates that the metal center is involved directly in the transport mechanism, this is not always the case.[41] Recent studies have highlighted the potential role of metal centers as a structural element

with the surrounding ligands providing the pathway for the through molecule current.[54] In such cases, the molecule-electrode contact and electronic structure of the ligand framework will play a more significant role in determining the overall transport properties of the molecule than the identity of the metal in the complex.

The important role of the molecule-electrode contact in determining transport properties of a molecular junction is now widely recognised,[55] and many different functional groups have been explored in this regard, with thiols, amines and pyridines being particularly widely used.[56] In addition to the chemical nature of the binding group, the electrode-molecule contact also depends on the structure of the electrode surface. For example, thiolate binds a wide variety of sites on the gold surface including different various points on flat terraces (atop surface atoms, in bridging or in hollow sites), adjacent step edges or ad-atoms.[57,58] Each of these different contact types gives rise to a different conductance signature, which accounts for the appearance of multiple peaks in the conductance histograms of even simple thiolate contacted molecules.[59] One possible strategy to limit the range of these possible binding sites, and thereby simplifying the conductance profile of the molecular junction, would entail increasing the steric bulk around the surface coordinating atom. Thioethers are beginning to attract attention in both studies of self-assembled monolayers (SAM) on gold,[60] and as a contact in molecular junctions where they often give rise to simpler conductance histograms than analogous thiolates.[61-66]

Recently, the trimethylsilylethynyl moiety has been identified as a possible 'bulky' anchoring moiety for use in single molecule electronics.[28,67-70] Results from single molecule junctions indicate that the use of the trimethylsilylethynyl moiety as surface contact group leads to current histograms containing only a single conductance peak in the measureable current range, although junction formation

probabilities are low (ca. 5%).[28,67] Detailed studies of SAM formed from trimethylsilylethynyl functionalised unsaturated hydrocarbons have indicated pit-etching features, consistent with a surprisingly strong Au-Si interaction.[71] A close registry of the silyl molecules with the underlying Au(111) surface and evidence for a degree of Si-Au interaction from synchrotron radiation photoelectron spectroscopy led to the suggestion of a local surface complex featuring a five-coordinate silicon atom in these self-assembled films.[72,73] Later refinements to the model have shown the importance of lateral intermolecular van der Waals interactions in pre-organising the silyl head group in such a position as to promote the Si-Au interaction.[74] However, the nature of the Si-Au interaction in the case of the isolated molecules used in single molecule junction studies is an area for further investigation.

In what follows, we seek to extend these studies and arrive at a more detailed understanding of the role of the anchor unit and metal complex fragment on the behaviour of these junctions, by studying Fe(II), Ru(II) and Co(II) bis-2,2′:6′,2″-terpyridine complexes anchored by thiomethyl[60-63] and trimethylsilylethynyl[28,67,68-70] moieties within molecular junctions, supported by electrochemical and spectroelectrochemical measurements and quantum chemical models.

**Results and Discussion**

The bis(terpyridyl) complexes [**1**-**M**]$(PF_6)_2$, [**2**-**M**]$(PF_6)_2$ and [**3**-**M**]$(PF_6)_2$ (M = Fe, Ru) (Chart 1) were prepared in conventional fashion from reactions of $FeCl_2.4H_2O$ or $RuCl_3.3H_2O$ (the latter in the presence of ethyl morpholine) with the ligands 4′-(trimethylsilylethynyl)-2,2′:6′,2″-terpyridine (**L**$^{\mathbf{1}}$),[75] 4′-[4-(trimethylsilylethynyl)phenyl]-2,2′:6′,2″-terpyridine (**L**$^{\mathbf{2}}$),[75] 4′-[4-(methylthio)phenyl]-2,2′:6′,2″-terpyridine (**L**$^{\mathbf{3}}$),[76] respectively, followed by anion metathesis with $NH_4PF_6$

or $[Ag(NCMe)_4]PF_6$. Whilst [**1-Co**]$(PF_6)_2$ could not be isolated, and indeed was not observed in ES-MS monitoring of analogous reactions of $[Co(H_2O)_6](BF_4)_2$ with $\mathbf{L^1}$, addition of $[Co(H_2O)_6](BF_4)_2$ to solutions of $\mathbf{L^2}$ or $\mathbf{L^3}$ readily gave [**2-Co**]$(BF_4)_2$ and [**3-Co**]$(BF_4)_2$. All of the complexes were characterised by the usual array of spectroscopic and spectrometric methods, and elemental analysis.

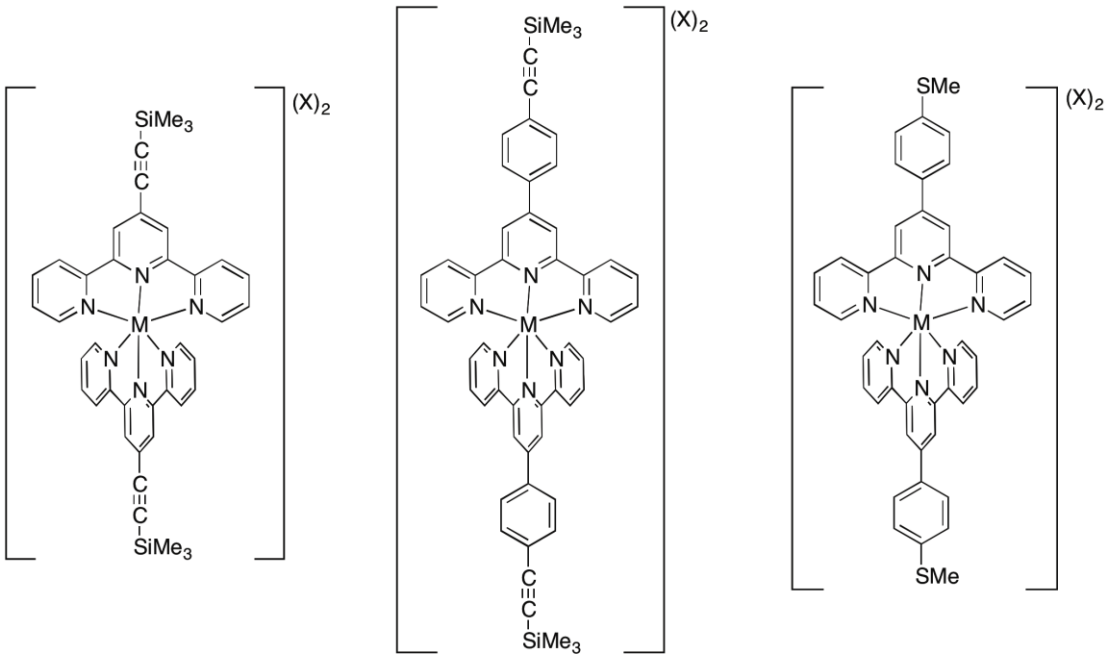


M = Fe, [**1-Fe**]$(PF_6)_2$
M = Ru, [**1-Ru**]$(PF_6)_2$

M = Fe, [**2-Fe**]$(PF_6)_2$
M = Ru, [**2-Ru**]$(PF_6)_2$
M = Co, [**2-Co**]$(BF_4)_2$

M = Fe, [**3-Fe**]$(PF_6)_2$
M = Ru, [**3-Ru**]$(PF_6)_2$
M = Co, [**3-Co**]$(BF_4)_2$

**Chart 1**

The complexes [**1-M**]$(X_2)$, [**2-M**]$(X)_2$ and [**3-M**]$(X)_2$ each undergo a metal-centered M(II/III) oxidation and two terpyridine based reduction processes (Table 1, Table S1), with assignments made on the basis of spectroelectrochemical studies (Table S2). In addition, the complexes [**2-Co**]$(BF_4)_2$ and [**3-Co**]$(BF_4)_2$ display a

metal-based Co(II/I) reduction at less negative potentials than the terpyridyl reductions (Table 1).

Interestingly, one-electron reduction products $[\mathbf{1\text{-}M}]^+$ and $[\mathbf{2\text{-}M}]^+$ display subtly different electronic characteristics, which can be conveniently assessed through IR spectroelectrochemical studies, using the ν(C≡C) and ν(tpy) reporting vibrations. Each of $[\mathbf{1\text{-}Fe}]^{2+}$ (ν(C≡C) 2164 $cm^{-1}$) and $[\mathbf{1\text{-}Ru}]^{2+}$ (ν(C≡C) 2162 $cm^{-1}$) feature a single ν(C≡C) band. The IR spectrum of the spectroelectrochemically observed one-electron reduction product $[\mathbf{1\text{-}Fe}]^+$ is characterised by the appearance of a new, strong ν(C≡C) band with an apparent maximum at 2111 $cm^{-1}$ together with a second ν(C≡C) band coincident with the ν(C≡C) band in $[\mathbf{1\text{-}Fe}]^{2+}$. These IR data are consistent with a $[Fe(\mathbf{L^1})([\mathbf{L^1}]^{\bullet-})]^+$ form which is localised on the IR timescale.[77] The reduction of $[\mathbf{1\text{-}Ru}]^{2+}$ to $[\mathbf{1\text{-}Ru}]^+$, which slowly decomposed in the course of the spectroelectrochemical experiment, resulted in a similar splitting (ν(C≡C) at 2161 and 2113 $cm^{-1}$). In the case of $[\mathbf{2\text{-}Fe}]^+$ and $[\mathbf{2\text{-}Ru}]^+$, the low-energy shifts, and size of the splitting of the ν(C≡C) bands were considerably smaller, resulting in the overlap of the new ν(C≡C) bands associated with $[\mathbf{2\text{-}Fe}]^+$ (2156, 2147 $cm^{-1}$) and a single ν(C≡C) band at 2150 $cm^{-1}$ for $[\mathbf{2\text{-}Ru}]^+$. Whilst close inspection of the entire NIR region of these 1-electron reduced complexes (through spectroelectrochemical experiments performed independently of the data presented in Figures S6, S9, S12, S15) failed to conclusively identify an interligand charge transfer transition, the observation of two ν(C≡C) bands in $[\mathbf{1\text{-}M}]^+$ and $[\mathbf{2\text{-}Fe}]^+$ suggests a localised terpyridyl reduction. In contrast, the observation of only a single ν(C≡C) band in $[\mathbf{2\text{-}Ru}]^+$ is consistent with fast electron exchange between the terpyridyl ligands on the IR time-scale.

The general conclusions drawn for the redox properties, molecular bonding and stability in the oxidized and reduced states presented above for the redox series based on $[\mathbf{2\text{-}M}]^{2+}$ can also be adopted for $[\mathbf{3\text{-}M}]^{2+}$. Only marginal differences between their redox potentials and electronic absorption spectra and those of $[\mathbf{2\text{-}M}]^{2+}$ have been encountered. Futher details of the analysis and copies of the spectra obtained by spectroelectrochemical methods are presented in Supporting Information (Figures S5 – S22, and Table S2).

To date, the few compounds featuring trimethylsilylethynyl based electrode contacts that have been studied in molecular junctions have been charge-neutral organic compounds[28,68-70,78] or organometallic complexes.[28] Therefore, prior to single-molecule measurements and by way of example, the deposition of the trimethylsilyl terminated complex $[\mathbf{2\text{-}Fe}](PF_6)_2$ on gold substrates from dilute acetonitrile solution was explored to ensure the trimethylsilylethynyl moiety would be capable of interacting with the gold substrate in the relatively highly charged coordination complexes studied here. A polished gold electrode was immersed in a solution of $10^{-3}$ M $[\mathbf{2\text{-}Fe}](PF_6)_2$ in acetonitrile and deposition allowed to proceed overnight. The modified electrode was rinsed with acetone and dried prior to use. Surface-enhanced resonance Raman spectroscopy ($\lambda_{ex}$ = 633 nm, chosen to be coincident with the plasmon absorption of a gold surface) revealed bands at 1044 and 1605 $cm^{-1}$, attributed to the tpy ligands, confirming attachment of $[\mathbf{2\text{-}Fe}](PF_6)_2$ to the surface (Figure S23). The surface bound complex showed a reversible anodic wave the shape of which was independent of scan rate up to 1 V $s^{-1}$ (Figure S24). The peak current of the anodic wave and cathodic counterwave scales linearly with increasing scan rate (Figure S25), whilst the corresponding peak-peak separation is ca. 25 mV and remains unaffected by changes of scan rate.

The molecular conductance of the bis-2,2′:6′,2″-terpyridine based complexes [**1-M**](X)$_2$ – [**3-M**](X)$_2$ (M = Fe, Ru, X = $PF_6^-$; M = Co, X = $BF_4^-$) on an Au(111) surface was investigated by scanning tunnelling microscopy (STM) under ambient conditions using the *I*(*s*) technique.[1] Approximately 500 *I*(*s*) scans containing current plateaus were used in the construction of the conductance histograms (Figure 1, Figure 2), from which the conductance, *G*, of the compounds under investigation can be extracted (Table 1). In addition, the break-off distance, *Z**, which is calculated from the sum of the initial separation of the tip and substrate ($s_0$) and the retraction distance defined by the end of the current plateau in the *I*(*s*) trace, can also be obtained from the conductance curves (Table 1). The relatively rigid junction between molecule and tip formed by both $Me_3SiC{\equiv}C$- and MeS- contacts was apparent from the observation of only short plateaus in the *I*(*s*) curves.[79] The conductance values, break-off distances and calculated molecular lengths are summarised in Table 1, with conductance histograms obtained from the *I*(s) data shown in Figure 1 and Figure 2.

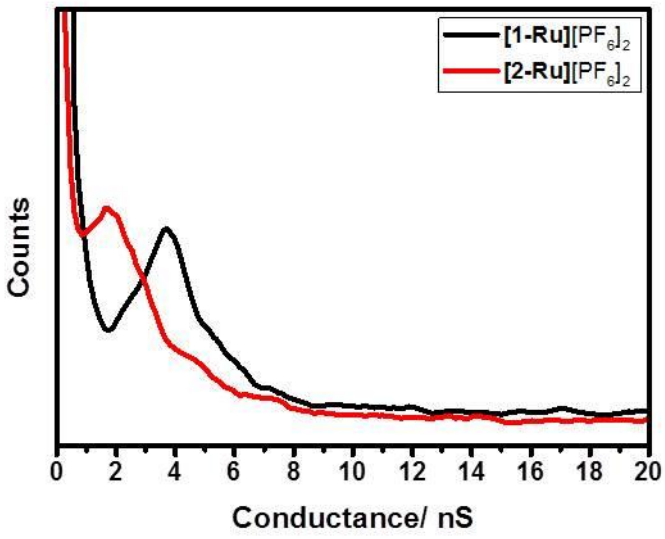


**Figure 1:** Conductance histograms of [**1-Ru**](PF$_6$)$_2$ and [**2-Ru**](PF$_6$)$_2$.

**Table 1:** The experimental (Exp. G) and calculated (Th. G) conductances, experimental break-off distances, and calculated geometric parameters from the Type III junction geometries (vide infra), with redox potentials[a] for complexes [**1-M**]$^{2+}$, [**2-M**]$^{2+}$ and [**3-M**]$^{2+}$ , recorded at $10^{-3}$ M in acetonitrile containing $10^{-1}$ M $NBu_4PF_6$.

| Molecule | Exp. G /nS ($G_0$)[b] | Th. G /nS ($G_0$)[c] | Z* /nm[d] | Z /nm[e] | $d_{Au\text{-}Au}$ /nm[f] | d /nm[g,h] | X /nm[i] | $E^1_{1/2}$ /V[j] | $E^2_{1/2}$ /V[k] | $E^3_{1/2}$ /V[l] | $E^4_{1/2}$ /V[m] |
|---|---|---|---|---|---|---|---|---|---|---|---|
| [**1-Fe**]$(PF_6)_2$ | 2.3±0.7 ((3.0±0.9)×$10^{-5}$) | | 2.0 | | | | | 0.77 | | -1.46 | -1.62 |
| [**1-Ru**]$(PF_6)_2$ | 3.7±1.0 ((4.8±1.3)×$10^{-5}$) | | 2.0 | | | | | 0.92 | | -1.49 | -1.73 |
| [**2-Fe**]$(PF_6)_2$ | 1.9±0.7 ((2.5±0.9)×$10^{-5}$) | 2.67 (3.45×$10^{-5}$) | 2.2 | 2.85 | 3.10 | 2.71[g] | 0.39 | 0.72 | | -1.56 | -1.68 |
| [**2-Ru**]$(PF_6)_2$ | 2.0±0.7 ((2.6±0.9)×$10^{-5}$) | 2.77 (3.58×$10^{-5}$) | 2.4 | 2.88 | 3.13 | 2.74[g] | 0.39 | 0.87 | | -1.58 | -1.83 |
| [**2-Co**]$(BF_4)_2$ | 1.4±0.6 ((1.8±0.8)×$10^{-5}$) | 1.95 (2.51×$10^{-5}$) | 2.7 | 2.83 | 3.08 | 2.69[g] | 0.39 | -0.08 | -1.08 | -1.92 | -2.25 |
| [**3-Fe**]$(PF_6)_2$ | 2.4±0.6 ((3.1±0.8)×$10^{-5}$) | 3.63 (4.69×$10^{-5}$) | 2.4 | 2.21 | 2.46 | 2.15[h] | 0.30 | 0.69 | | -1.60 | -1.73 |
| [**3-Ru**]$(PF_6)_2$ | 2.4±0.6 ((3.1±0.8)×$10^{-5}$) | 3.28 (4.23×$10^{-5}$) | 2.4 | 2.24 | 2.49 | 2.19[h] | 0.30 | 0.83 | | -1.64 | -1.87 |
| [**3-Co**]$(BF_4)_2$ | 4.1±1.0 ((5.3±1.3)×$10^{-5}$) | 5.60 (7.23×$10^{-5}$) | 2.0 | 2.20 | 2.45 | 2.14[h] | 0.30 | -0.10 | -1.14 | -1.96 | -2.30 |

[a]The electrode potentials of the Fe(II) and Ru(II) complexes were internally referenced against $FeCp_2/[FeCp_2]^+$ at $\nu$ = 100 mV $s^{-1}$, while the Co(II) complexes were internally referenced against decamethylferrocene/decamethylferrocenium ($FeCp^*_2/[FeCp^*_2]^+$ = −0.48 V vs $FeCp_2/[FeCp_2]^+$) at $\nu$ = 1 V $s^{-1}$. The same half-wave potentials were recorded in butyronitrile used for IR spectroelectrochemistry due to higher solubility of the complexes. [b] Experimentally determined conductance G (nS). [c] Calculated conductance values Th. G (nS) at $E_F - E_F^{DFT}$ = –0.14 eV. [d] experimental break-off distance Z* (nm). [e] The calculated electrode separation in a relaxed Type III junction, Z = $d_{Au\text{-}Au}$ – 0.25 nm, where 0.25 nm is the calculated center-to-center distance of the apex atoms of the two opposing gold pyramids when conductance = $G_0$ in the absence

of a molecule. [f] $d_{Au-Au}$ is the calculated center-to-center distance of the apex atoms of the two opposing gold pyramids in the relaxed Type III junctions (vide infra). [g] Distance between the centres of silicon atoms in the relaxed junction. [h] Distance between centres of sulfur atoms in the relaxed junction. [i] Bond length between the top gold atoms of the pyramids and the anchor atoms in the relaxed junctions. [j] Metal-centred oxidation. [k] Metal-centred reduction. [l] Ligand-based reduction. [m] Second ligand based reduction.

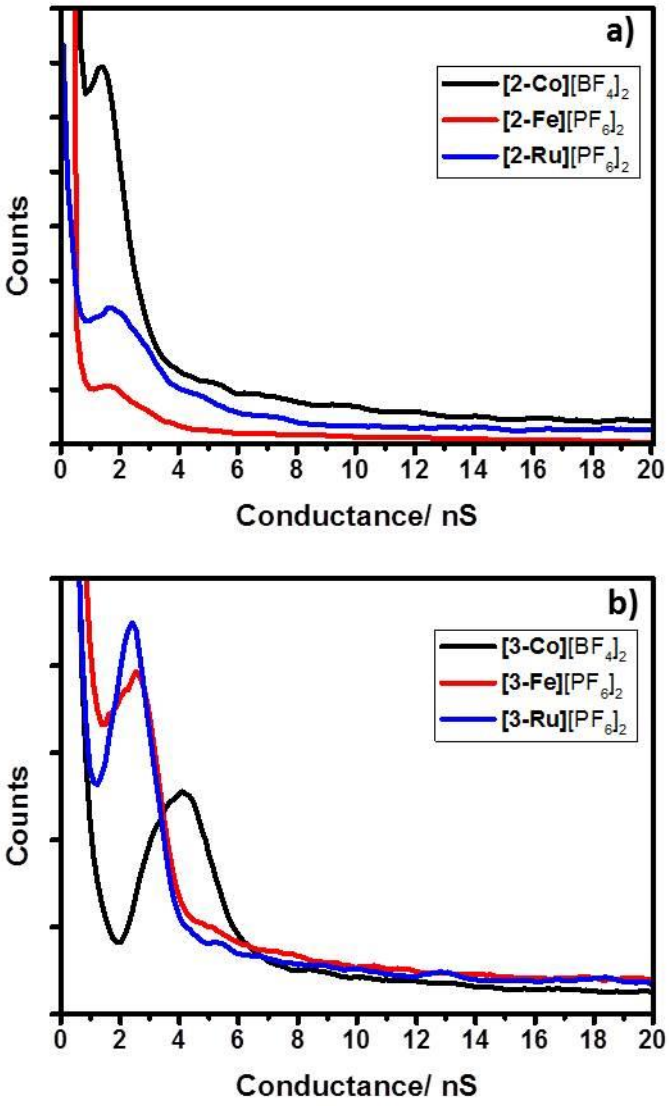


**Figure 2:** Conductance histograms. (a) -C≡CSiMe$_3$ contacted complexes [**2-Fe**](PF$_6$)$_2$, [**2-Co**](BF$_4$)$_2$ and [**2-Ru**](PF$_6$)$_2$. (b) -SMe contacted complexes [**3-Fe**](PF$_6$)$_2$, [**3-Co**](BF$_4$)$_2$ and [**3-Ru**](PF$_6$)$_2$.

The data in Table 1 is consistent with literature studies of OPEs and oligoynes, whose tunnelling conductances decay with increasing numbers of phenyl rings and triple bonds respectively, one expects the conductances of [**2-M**](X)$_2$ to be lower than that of [**1-M**](X)$_2$ and [**3-M**](X$_2$), because each end of [**2-M**](X)$_2$ contains both a

phenylene and a triple bond in series, where each end of [**1-M**](X)$_2$ and [**3-M**](X$_2$) contain only a single phenylene spacer or a single triple bond respectively. There are several competing factors here, including the increased molecular length (β for polyphenylene chains is said to be 0.6 A$^{-1}$)[80] and the decreased conjugation brought about by the twisting of the phenylene ring relative to the plane of the tpy π-system.[81,82] Whilst for each series [**2-M**]$^{2+}$ and [**3-M**]$^{2+}$ the overall span of values is not more than a factor of three (Table 1, Figure 2), the apparent order of conductance is Ru ≥ Fe > Co for the trimethylsilylethynyl contacted complexes [**2-M**]$^{2+}$, whilst for the MeS derivatives [**3-M**]$^{2+}$ a trend of Co > Fe ≥ Ru is observed. However, there is no correlation between the trends in solution-based redox potentials and the observed conductance behaviour (Table 1), which may be an indication of non-resonant transport mechanisms. The relative energies of the gold electrode Fermi energies and the molecular redox states (or energies of the HOMO and LUMO orbitals) are not readily estimated with significant accuracy as the electrochemical potentials (Table 1) will depend on experimental factors such as solvation and ion-pairing, and the effects of the double layer at the (electrochemical) electrode surface. In contrast, the STM experiments are based on two-terminal (STM tip and substrate) measurements in which the electrochemical potential is not controlled. In this case the STM tip and substrate operate with a bias between them ($U_{tip}$ = 0.6 V) and the precise level relative to vacuum depends on the open circuit potentials adopted.

Therefore, to further explore the properties of these molecular junctions, quantum chemical modeling of the complete junctions were undertaken to compare the electrical properties of the Fe, Ru and Co molecular pairs [**2-M**](X)$_2$ and [**3-M**](X)$_2$ (M = Fe, Ru, X = $PF_6^-$; M = Co, X = $BF_4^-$) (Figure 3).

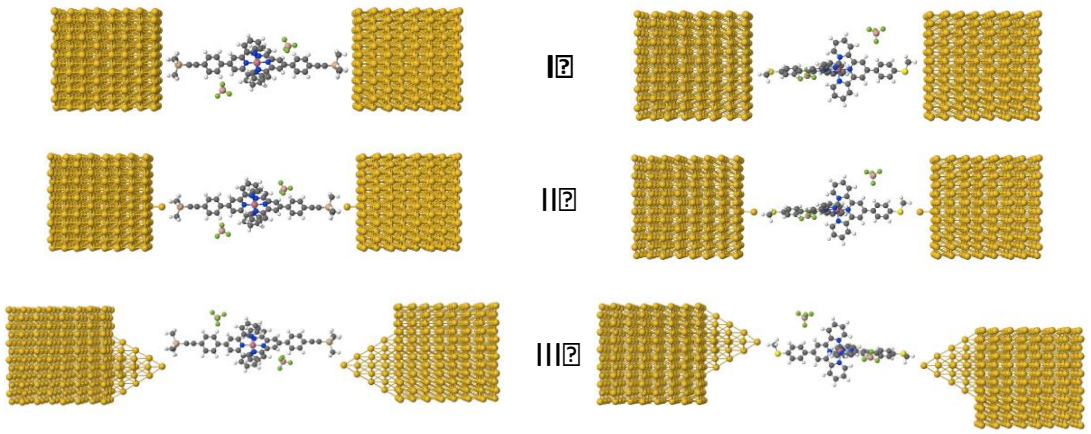

**Figure 3:** The three distinct electrode geometries were explored, denoted Type I, Type II and Type III. By way of example, this figure shows [**2-Co**]$(BF_4)_2$ and [**3-Co**]$(BF_4)_2$ located between electrodes with the three chosen geometries (see Figures S31, S32, S33 for all relaxed structures).

Before calculating electron transport properties, each member of the [**2-M**]$(X)_2$ and [**3-M**]$(X)_2$ series was optimized within the junctions. (Figure 3). To explore the role of the electrode geometry, three electrode shapes were chosen to represent not only the idealized planar surface (Type I), but also surfaces containing a single adatom (Type II) and larger surface features modeled as gold pyramids (Type III). To obtain realistic values of molecular conductance for the Type III junctions with a $Me_3SiC{\equiv}C$- anchor group, the binding energies of these structures were computed for a range of different molecular orientations within the junction (defined by the angle Θ, $\angle C_{ipso}$-Si-Au, Figure 4).

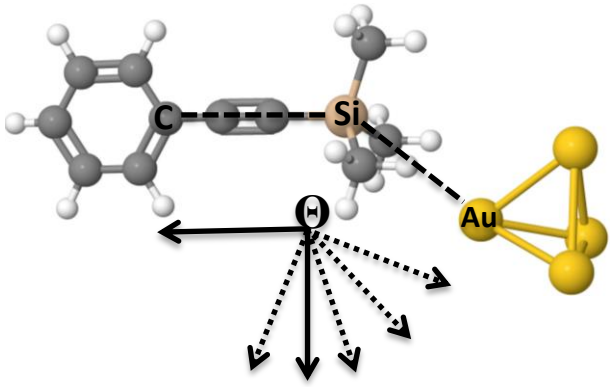


**Figure 4:** A pictorial representation of the angle Θ used to describe the various geometries within Type III junctions for complexes [**2-M**]$^{2+}$.

Within this range of different conformations of Type III junctions, the maximum binding energy varied by about 0.1 eV from 105 º to 125 º depending on the metal ion involved (Figure 5). Allowing for room-temperature thermal fluctuations of ~25 meV, this suggests that the optimal conformation of the angle Θ within the junction may vary from as little as 100 º for [**2-Co**] to as much as 130 º for [**2-Fe**] and [**2-Ru**]. However, since the results do not depend strongly on the angle, we have chosen to plot results for the case of Θ = 110º as a representation of the results for a range of nearby angles. Results for binding energies (Figure 6) and transport properties (vide infra) are shown for Type III junctions with Θ = 110°.

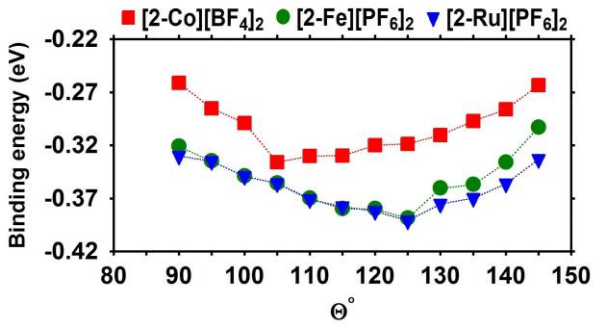


**Figure 5:** Plots illustrating the binding energies as a function of the angle between Au-Si-C atoms, Θ, (Figure 4) for the Type III configurations with the $Me_3SiC{\equiv}C$ anchored compounds [**2-M**]$(X)_2$.

Calculated binding energies for the various complexes [**2-M**]$(X)_2$ and [**3-M**]$(X)_2$ in various junction models I, II, III (Θ = 110º) are plotted in Figure 6, with two trends immediately apparent. Firstly, the MeS-based structures ([**3-M**]$^{2+}$) bind more strongly than the $Me_3SiC{\equiv}C$-anchored structures ([**2-M**]$^{2+}$). Secondly, the binding energies of the Type III electrode geometry are higher than the other junctions. For these Type III junctions, the order of the binding energies with $Me_3SiC{\equiv}C$-anchor groups ([**2-M**]$X_2$) is Ru > Fe > Co, whereas with MeS-anchor groups (i.e. compounds [**3-M**][$X]_2$), the order of binding energies is Co > Fe > Ru, which are broadly consistent with the conductance trends.

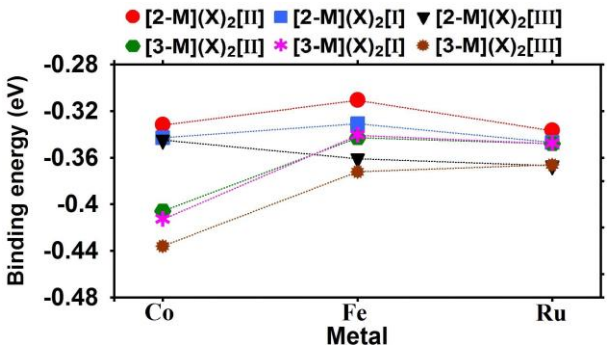


**Figure 6:** Plots of the binding energy of [**2-M**](X)$_2$ and [**3-M**](X)$_2$ for three types of junction configurations, Type I, Type II and Type III.

The most stable trimethylsilylethynyl-based configurations in the single-molecule junctions formed with complexes [**2-M**]$^{2+}$ are not as might have been expected based on previous proposals drawn from studies of self-assembled monolayers of trimethylsilylethynyl functionalized long-chain hydrocarbons on flat Au(III) surfaces.[71,72,74,83] Rather than a five-coordinate silicon species chemisorbed to a flat terrace, the Type III junctions are most stable, and the silicon centre maintains an approximately tetrahedral geometry (Table 2). It seems that for the single-molecule experiments, in the absence of additional dispersion forces present in the self-assembled mono-layer films, which might give additional energetic preference to alternative contact geometries,[71-74] the most stable trimethylsilylethynyl | gold contacts are best described in terms of a molecule physisorbed at a defect site.

**Table 2:** Summary of bond lengths (Å) and angles at Si (º) of the dication [**2-M**]$^{2+}$ in Type III junctions.

| | Type III junction | | |
|---|---|---|---|
| | [**2-Fe**]$^{2+}$ | [**2-Ru**]$^{2+}$ | [**2-Co**]$^{2+}$ |
| C≡C | 1.234 | 1.234 | 1.234 |
| Si-C≡ | 1.824 | 1.825 | 1.819 |
| Si-$C_{methyl}$ | 1.907 | 1.887 | 1.889 |
| ∠$C_{methyl}$-Si-$C_{alkyne}$ | 109.7 | 109.1 | 109.3 |

Regarding the relaxed geometries of the molecular junctions formed by the SMe contacted molecules [**3-M**]$(X)_2$, we note that whilst the thiolate ($RS^-$) to gold interaction has been studied extensively,[84,54] the thioether ($R_2S$) to gold interaction has been less thoroughly explored. In the Type III contacted thioether systems, the compounds [**3-M**]$^{2+}$ sit close to the apex of each pyramid-shaped model gold electrode, with a Au-S distance of 2.41 Å, and an Au-S-$C_{ipso}$ angle of 103.74 º. These geometries compare with compounds such as $[Ph_3PAuSMe_2][CF_3SO_3]$ (Au-S, 2.323(2) Å; Au-S-$C_{methyl}$ 106.7(2), 104.7(2) º),[85] and as such the sulfur-gold interaction is well approximated in terms of a coordination-type interaction (chemisorption) between the sulfur donor atom of the thio-ether and the gold atoms near the apex of the pyramid.

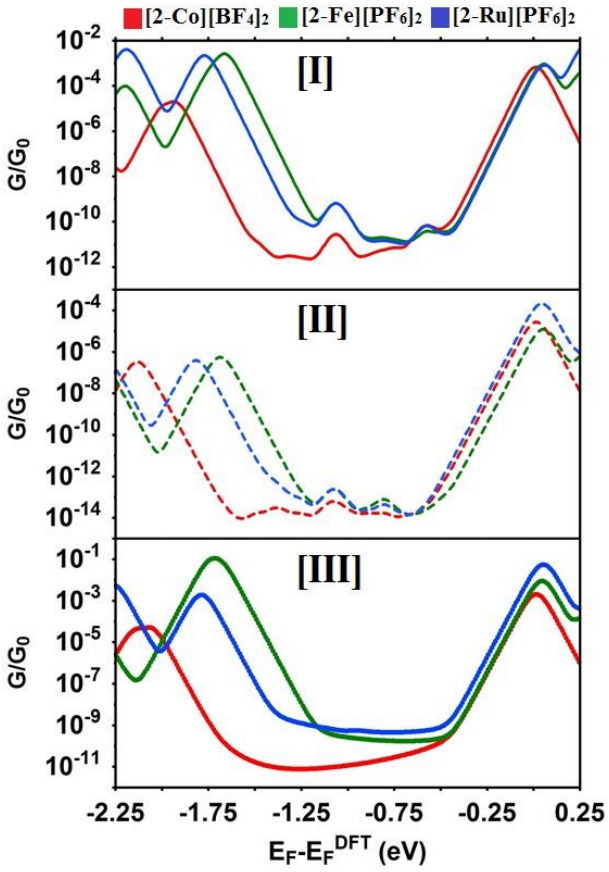


**Figure 7:** Plots of the theoretical conductances as a function of the Fermi energy for [**2-M**](X)$_2$ with three different molecular junctions (Type I, II, III).

The calculated conductances as a function of the Fermi energy for complexes [**2-M**](X)$_2$ and [**3-M**](X)$_2$ within the three different molecular junctions Type I, II and III are shown in Figures 7 and 8. For both molecular contacts, it is clear the conductances of the structures with the Type III configurations are the highest, which correlates with their more favourable binding energies (Figure 6). This is consistent with the relatively simple conductance histograms observed for trimethylsilylethynyl and SMe contacted molecules described here and elsewhere,[28,61-63] and might be attributed to molecules bound at surface defects contributing predominantly to the conductance histograms.

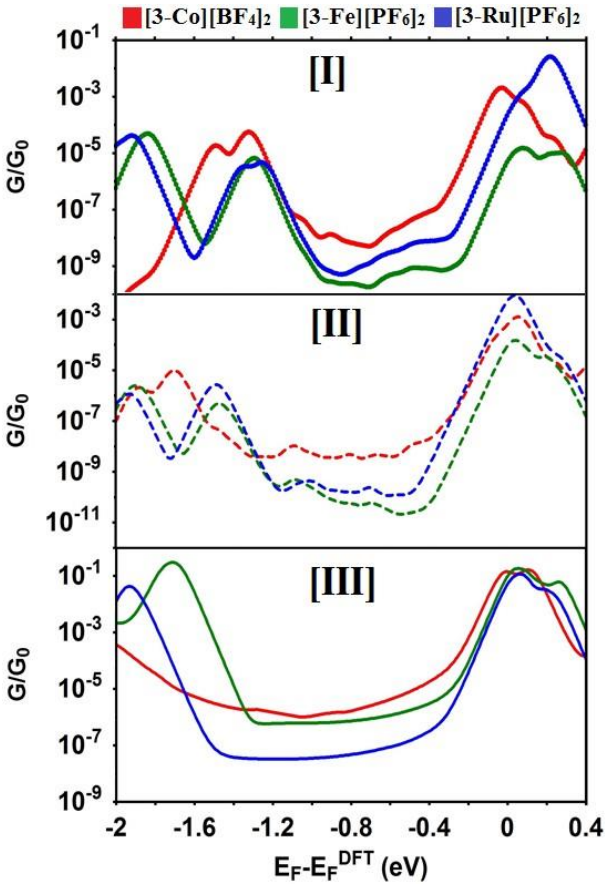


**Figure 8:** Plots of the theoretical conductance as a function of the Fermi energy for all [**3-M**](X)$_2$ structures with three different molecular junctions (Type I, II, III).

For each of the most energetically favorable Type III structures of [**2-M**](X)$_2$ and [**3-M**](X)$_2$, the room temperature electrical conductance *G* was calculated as described in the computational methods section, and plotted against the Fermi level ($E_F$-$E_F^{DFT}$) (Figure 7, Figure 8). Since DFT does not usually predict the correct value of the Fermi energy ($E_F^{DFT}$), we treat $E_F$ as a free parameter which we determine by comparing the calculated conductance with experiment. For $E_F$ - $E_F^{DFT}$ = - 0.14 eV, the conductances follow the small experimental trends with remarkably high degree of correlation (Table 1, Figure 9). Thus, despite the changes in metal and surface contacting group, the observed conductances of these metal complexes, which span a relatively small range of values (from (1.4 ± 0.6) – (4.1 ± 1.0) nS, Table 1), follow the

trends in the edge of the LUMO resonances (Figures 7, 8). In contrast, there is a more pronounced variation in the position of the HOMO resonances, but such variations are not consistent with the conductance data. LUMO-based conduction mechanisms have also recently been noted for a somewhat related Cu(phenanthroline) complex.[41] Interestingly, a family of SMe contacted oligo(thiophene-*S*,*S*-dioxides) have been shown to shift from LUMO to HOMO mediated conductance mechanisms as a function of increasing molecular length.[62]

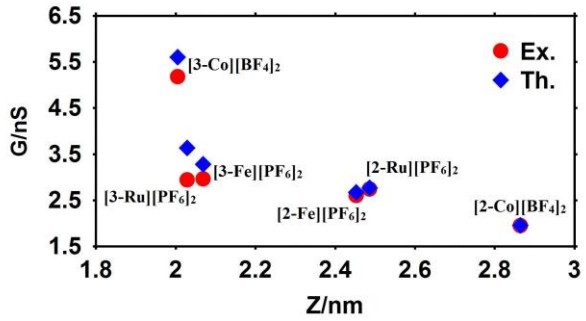


**Figure 9:** A comparison between experimental and theoretical conductances *G*, plotted against the relaxed electrode separations Z as shown in Table 1.

## CONCLUSIONS

The single-molecule conductance of bis(terpyridyl) complexes [**1**-**M**]$(X)_2$, [**2**-**M**]$(X)_2$ and [**3**-**M**]$(X_2)$ display trends that are more closely associated with the binding energy and ligand structure than the nature of the metal ion. The limited role of the metal ion can be traced in part to the LUMO-based conduction mechanisms that arise from the use of trimethylsilylethynyl and, in the geometries adopted here, thiomethyl binding groups. The optimised structures of the molecular junctions and considerations of the calculated conductance profiles indicate that the most conductive trimethylsilylethynyl contact to the gold electrodes is best described in

terms of physisorption at defect sites, explaining the simple conductance profiles observed for compounds contacted through this group. The thiomethyl moiety contacts the gold electrodes in a more chemisorbed fashion, again at defect sites on the gold electrodes in the most conductive junctions. The conductances of [**2**-**M**]$(X)_2$ are found to be lower than those of [**1**-**M**]$(X)_2$ and [**3**-**M**]$(X_2)$, which is consistent with single phenylene and triple-bond spacers acting as tunneling barriers.

## Experimental

*General details.* NMR spectra were recorded in deuterated solvent solutions on Bruker DRX-400 and Varian Inova 300, 400, 500 spectrometers and referenced against residual protio solvent resonances ($^1$H, $^{13}$C). ES-MS data were recorded on a TQD mass spectrometer (Waters Ltd, UK) in acetonitrile. Microanalyses were performed by Elemental Analysis Service, London Metropolitan University, UK.

Analytical grades of solvents were used except for dichloromethane ($CH_2Cl_2$), which was further purified by distillation over calcium hydride. The compounds 4′-(trimethylsilylethynyl)-2,2′:6′,2″-terpyridine (**L**$^{\mathbf{1}}$),[75] 4′-[4-(trimethylsilylethynyl)phenyl]-2,2′:6′,2″-terpyridine (**L**$^{\mathbf{2}}$),[75] 4′-[4-(methylthio)phenyl]-2,2′:6′,2″-terpyridine (**L**$^{\mathbf{3}}$),[76] [Ru(**L**$^{\mathbf{3}}$)$_2$]$(PF_6)_2$ ([**3**-**Ru**]$(PF_6)_2$)[76] and $[Ag(CH_3CN)_4]PF_6$[86] were synthesised according to literature methods. All other chemicals were purchased and used as received.

*Syntheses.*

*[Fe(**L**$^{1}$)$_2$](PF$_6$)$_2$* (***[1-Fe](PF$_6$)$_2$***). The salt $FeCl_2 \cdot 4H_2O$ (60 mg, 0.30 mmol) was added to a solution of **L**$^{1}$ (200 mg, 0.60 mmol) in methanol (20 mL), immediately turning the solution purple. The reaction mixture was stirred for 30 min, then solvent was removed leaving a purple residue, which was then dissolved in acetonitrile (20 mL). To this solution, $[Ag(CH_3CN)_4]PF_6$ (249 mg, 0.60 mmol) was added forming a white precipitate, which was removed via filtration through Celite. The solvent was removed from the filtrate leaving a purple residue, which was dissolved in $CH_2Cl_2$ (20 mL) and precipitated by adding a minimal amount of hexane. The supernatant was removed by decantation, and the remaining purple oil was washed with hexane twice before being dried under high vacuum to give a purple solid. Yield: 150 mg (49 %). ESMS: *m/z* 357 $[M]^{2+}$. $^{1}$H NMR($CD_3CN$): δ 8.94 (s, 4H), 8.48 (d (J = 8 Hz), 4H), 7.90 (t (J = 8 Hz), 4H), 7.13-7.07 (m, 8H), 0.46 (s, 18H) ppm. $^{13}C\{^{1}H\}$ NMR ($CD_3CN$): δ. 161.1, 158.1, 154.1, 139.9, 133.0, 128.5, 126.4, 125.0, 105.6, 102.0, -0.42 ppm. Anal. Calc. for $C_{40}H_{38}F_{12}FeN_6P_2Si_2$: C, 47.82; H, 3.81; N, 8.36 %. Found: C, 47.75; H, 3.73; N, 8.27 %.

*[Ru(**L**$^{1}$)$_2$](PF$_6$)$_2$* (***[1-Ru](PF$_6$)$_2$***). The complex salt $RuCl_3 \cdot 3H_2O$ (78 mg, 0.30 mmol), **L**$^{1}$ (200 mg, 0.60 mmol) and 5 drops of ethyl morpholine in methanol (20 mL) were heated at reflux for 6 hours, after which time the solution was allowed to cool to room temperature and filtered. The solvent was removed from the filtrate leaving a red residue. The residue was re-dissolved in acetonitrile, and $[Ag(CH_3CN)_4]PF_6$ (313 mg, 0.75 mmol) was added, forming a white precipitate, which was removed by filtration through Celite. The solvent was removed from the filtrate forming a red solid, which was dissolved in $CH_2Cl_2$, filtered and the filtrate subjected to silica

column chromatography eluted with $CH_2Cl_2$:acetonitrile (1:1). The red band was collected, and removal of the solvent gave the product as a red solid. Yield: 50 mg (15%). ESMS: *m/z* 380 $[M]^{2+}$. $^1$H NMR($(CD_3)_2CO$): δ 9.10 (s, 4H), 8.92 (d (J = 8 Hz), 4H), 8.09 (t (J = 8 Hz), 4H), 7.80 (d (J = 8 Hz), 4H), 7.35 (t (J = 8 Hz), 4H), 0.40 (s, 18 H) ppm. $^{13}C\{^1H\}$ NMR ($(CD_3)_2CO$): δ 158.7, 156.4, 153.7, 139.4, 131.2, 129.0, 126.8, 125.9, 104.1, 102.5, -0.21 ppm. Anal. Calc. for $C_{40}H_{38}F_{12}RuN_6P_2Si_2$: C, 45.76; H, 3.65; N, 8.00 %. Found: C, 45.65; H, 3.77; N, 7.94.

*[Fe(**L**$^2$)$_2$](PF$_6$)$_2$* (***[2-Fe](PF$_6$)$_2$***). The complex was prepared using the same procedure as described for [**1-Fe**]$(PF_6)_2$ except $\mathbf{L}^2$ was used in place of $\mathbf{L}^1$. Yield: 142 mg (63%). ESMS: *m/z* 433 $[M]^{2+}$. $^1$H NMR($CD_3CN$): δ 9.19 (s, 4H), 8.63 (d (J = 8 Hz), 4H), 8.34 (d (J = 8 Hz), 4H), 7.93 (t (J = 8 Hz), 4H), 7.88 (d (J = 8 Hz), 4H), 7.20 (d (J = 7 Hz), 4H), 7.10 (t (J = 7 Hz), 4H), 0.35 (s, 18H) ppm. $^{13}C\{^1H\}$ NMR ($CD_3CN$): δ. 161.3, 158.9, 154.0, 150.2, 139.7, 137.7, 133.8, 129.0, 128.3, 126.1, 124.8, 122.4, 105.0, 98.0, -0.16 ppm. Anal. Calc. for $C_{52}H_{46}N_6F_{12}P_2FeSi_2$: C, 53.99; H, 4.01; N, 7.26 %. Found: C, 53.71; H, 4.09; N, 7.17%.

*[Co(**L**$^2$)$_2$](BF$_4$)$_2$* (***[2-Co](BF$_4$)$_2$***). The complex salt $Co(BF_4)_2 \cdot 6H_2O$ (85 mg, 0.25 mmol) was added to a solution of $\mathbf{L}^2$ (200 mg, 0.49 mmol) in $CH_2Cl_2$ (10 mL) and methanol (5 mL), immediately forming a red solution. The solution was allowed to stir for 30 min, before the solvent was removed leaving a red solid that was dissolved in $CH_2Cl_2$ and the resulting solution filtered through Celite. The solvent was removed from the filtrate giving the product as a red solid. Yield: 212 mg (83%). ESMS: m/z 435 $[M]^{2+}$. Anal. Calc. for $C_{52}H_{46}B_2F_8CoN_6Si_2 \cdot ½CH_2Cl_2$: C, 58.06; H, 4.36; N, 7.74 %. Found: C, 58.13; H, 4.19; N, 7.47 %.

*[Ru(**L**$^{2}$)$_2$](PF$_6$)$_2$* (***[2-Ru](PF$_6$)$_2$***).This complex was prepared using the same procedure as described for [**1-Ru**](PF$_6$)$_2$ except **L**$^{2}$ was used in place of **L**$^{1}$. Yield: 174 mg (29%). ESMS: m/z 456 [M]$^{2+}$. $^{1}$H NMR(CD$_3$CN): δ 9.02 (s, 4H), 8.67(d (J = 8 Hz), 4H), 8.23 (d (J = 8 Hz), 4H), 7.97 (t (J = 8 Hz), 4H), 7.45 (d (J = 8 Hz), 4H), 7.20 (d (J = 7 Hz), 4H), 7.10 (t (J = 7 Hz), 4H), 0.33 (s, 18H). $^{13}$C{$^{1}$H} NMR (CD$_3$CN): δ. 159.0, 156.4, 153.4, 148.0, 143.2, 139.0, 137.8, 133.7, 128.9, 128.4, 125.5, 122.4, 105.0, 97.7, -0.17 ppm. Anal. Calc. for C$_{52}$H$_{46}$N$_6$F$_{12}$P$_2$RuSi$_2$: C, 51.95; H, 3.86; N, 6.99 %. Found: C, 51.84; H, 4.02; N, 6.80 %.

*[Fe(**L**$^{3}$)$_2$](PF$_6$)$_2$* (***[3-Fe](PF$_6$)$_2$***). The complex salt FeCl$_2$·4H$_2$O (55 mg, 0.28 mmol) was added to a solution of **L**$^{3}$ (200 mg, 0.56 mmol) in CH$_2$Cl$_2$ (10 mL) and methanol (10 mL), immediately forming a purple solution. The reaction mixture was stirred for 30 min, after which time the solvent was removed *in vacuo* before being redissolved in neat methanol. Addition of NH$_4$PF$_6$ (137 mg, 0.84 mmol) resulted in the formation of a precipitate. The precipitate was collected by filtration and washed thoroughly by methanol, followed by CH$_2$Cl$_2$ and finally diethyl ether. The combined filtrates were taken to dryness, giving the product as a purple powder. Yield: 215 mg (73 %). ESMS: *m/z* 383 [M]$^{2+}$. $^{1}$H NMR(CD$_3$CN): δ 9.19 (s, 4H), 8.64 (d (J = 8 Hz), 4H), 8.29 (d (J = 8 Hz), 4H), 7.93 (t (J = 8 Hz), 4H), 7.70 (d (J = 8 Hz), 4H), 7.22 (d (J = 6 Hz), 4H), 7.11 (t (J = 6 Hz), 4H), 2.69 (s, 6H). $^{13}$C{$^{1}$H} NMR (CD$_3$CN): δ. 160.2, 158.0, 153.0, 149.7, 143.0, 138.6, 132.6, 128.1, 127.2, 126.4, 123.7, 121.0, 14.2 ppm. Anal. Calc. for C$_{44}$H$_{34}$N$_6$F$_{12}$P$_2$FeS$_2$: C, 50.01; H, 3.24; N, 7.95 %. Found: C, 49.83; H, 3.16; N, 7.85 %.

*$[Co(\mathbf{L^3})_2](BF_4)_2$* (***[3-Co]$(BF_4)_2$***). The complex was prepared using the same procedure as described above for [**2-Co**]$(BF_4)_2$ except $\mathbf{L^3}$ was used in place of $\mathbf{L^2}$. Yield: 213 mg (81 %). ESMS: m/z 385 $[M]^{2+}$. Anal. Calc. for $C_{44}H_{34}N_6F_8B_2CoS_2$: C, 56.02; H, 3.63; N, 8.91 %. Found: C, 55.97; H, 3.55; N, 9.07 %.

*Single molecule conductance measurements***.** Gold on glass substrates (Arrandee, Schröer, Germany) were cleaned with acetone and flame-annealed with a butane torch until a slight orange hue was obtained. The slide was kept in this state for 20 seconds during which time the torch was kept in motion around the sample to avoid overheating. This procedure was performed three times to generate flat Au (111) terraces.[87] The freshly annealed substrates were immersed in a $10^{-4}$ M acetonitrile (99.9% ChromasolV Plus for HPLC) solution of the complex under investigation for 1 minute, after which time the gold sample was removed and washed with ethanol and then dried in an argon flow. The short immersion time and low concentration of solution were chosen to promote low molecular coverage of the gold surface, which increases the formation of single molecule events over aggregate phenomena.

Conductance values of those compounds and the break off-distance were obtained with a STM (Agilent 5500 SPM microscope), using the *I*(*s*) technique in which an electrochemically etched gold tip is approached close to the substrate surface and then retracted with the tunnelling current (*I*) recorded against distance (*s*).[88] The Agilent 5500 SPM fitted was fitted with a low-current preamplifier and set point conditions of $I$ = 10 nA and bias voltage, $U_{tip}$ = 0.6 V were employed. The *I*(*s*) method involves repeatedly moving the STM tip towards the gold surface to given set-point values and then rapidly away from the surface. During these cycles molecular junctions are occasionally formed which can be recognized by deviations from the usual

exponential decay of current in the form of current plateaus. In this case as the junction is stretched beyond its maximum length, the molecule bridge breaks, leading to a sharp decrease in current and currents steps. Hence these junction formation and cleavage processes are recognized by plateaus and steps in the current-distance currents. Since the *I*(*s*) technique is a "non-contact" method (no metallic contact between the gold STM tip and gold surface) the molecular junction formation probability, as recognized by the plateau-step traces, is significantly smaller than break junction techniques. The *I*(*s*) tip retraction cycles are repeated many times (normally 4000-5000 traces) in order to record sufficient traces where molecular junctions form, called molecular junction formation scans, as opposed to most traces for which no junction forms. Molecular junction formation scans are recognized by recording only traces which exhibit a plateau longer than 1 Å. This accounted for ~15% of the current decay curves for the molecules with SMe anchor group but as low as 1% for the TMSE end groups (Figure S36). The very low hit rate for the TMSE terminal groups may be related to either their relatively weak contact binding or possibly their propensity to bind as only specific surface defects sites (e.g. gold steps) with sufficient conductance. The resulting *I*(*s*) curves are binned in current steps (16 pS) and plotted to give a conductance histogram comprised of at least 500 *I*(*s*) scans showing plateaus. The error associated with each current value reported has been statistically obtained from the standard deviation of the points comprising the conductance peak.

*Spectroelectrochemistry.* UV-Vis-NIR spectroelectrochemistry was conducted using a Scinco S-3100 diode array spectrophotometer (50000-10000 $cm^{-1}$) or a Perkin-Elmer Lambda 900 double-beam spectrophotometer (50000-5000 $cm^{-1}$). An optically

transparent thin-layer electrochemical (OTTLE) cell[89] was connected to a PalmSens EmStat3 potentiostat. Infrared spectra were recorded with a Bruker Vertex 70v spectrometer. All spectroelectrochemical experiments were conducted in pre-dried solvents (acetonitrile, butyronitrile) containing $3\times10^{-1}$ M $NBu_4PF_6$ and $10^{-3}$ M complex (UV-Vis-NIR monitoring) or $10^{-2}$ M complex (IR monitoring).

*Deposition of [**2-Fe**](PF$_6$)$_2$ on Au Microdisc Electrode Surface.* In order to deposit [**2-Fe**](PF$_6$)$_2$ on a gold disc microelectrode ($d$ = 0.4 mm), the electrode surface was polished by hand on polishing pads, using MasterPrep polishing solution (0.5 μM alumina). It was then sonicated for 15 min to remove any adsorbed alumina particles prior to electrochemical cleaning. Diluted sulfuric acid (0.5 M) was placed into a standard electrochemical cell fitted with a silver wire pseudoreference electrode, platinum wire counter electrode and the polished gold microdisc working electrode. Twenty CV cycles were then run to clean the gold surface. After cleaning, the standard three electrode cell was refilled with the acetonitrile/$10^{-1}$ M $NBu_4PF_6$ electrolyte and a 'blank' CV scan was run to prove that the gold surface was clean prior to deposition. The polished gold electrode was submerged into a solution of $10^{-3}$ M [**2-Fe**](PF$_6$)$_2$ in acetonitrile and left overnight; after the deposition it was rinsed with acetone and dried.

*Resonance Raman Spectroscopy.* The cleaned and polished Au microdisc electrode modified by deposition of [**2-Fe**](PF$_6$)$_2$ on the surface was used for the resonance Raman spectroscopy. The electrode was rinsed with acetone and dried before use to remove any molecules of [**2-Fe**](PF$_6$)$_2$ that were not adsorbed onto the gold surface.

Resonance Raman spectra were recorded on a Renishaw inVia Raman microscope, using a 633-nm laser beam focused into the middle of the gold microdisc.

**Computational details**

Geometrical optimizations were carried out using the DFT code SIESTA, with a generalized gradient approximation (PBE functional),[90] double-zeta polarized basis set, 0.01 eV/A force tolerance, a real-space grid with a plane wave cut-off energy of 250 Ry, zero bias voltage and 1 k points. To compute the electrical conductance of the molecules, they were each placed between pyramidal gold electrodes. The complex cations and their associated counter ions were then placed in the vicinity of the metal | molecule | metal junctions. The complexes and the first few layers of gold were again allowed to relax, to yield the structures shown in Figures 3, S31, S32 and S33. For each structure, the transmission coefficient *T(E)* describing the propagation of electrons of energy *E* from the left to the right electrode was calculated by first obtaining the corresponding Hamiltonian and overlap matrices using SIESTA[91] and then using the GOLLUM code[92] to compute *T(E)* via the relation

$$T(E) = Trace\{\Gamma_R(E) G^R(E) \Gamma_L(E) G^{R\dagger}(E)\}$$

In this expression, $\Gamma_{L,R}(E) = i\left(\sum_{L,R}(E) - \sum_{L,R}{}^{\dagger}(E)\right)$ describes the level broadening due to the coupling between left (L) and right (R) electrodes and the central scattering region, $\sum_{L,R}(E)$ are the retarded self-energies associated with this coupling and $G^R = (ES - H - \sum_L - \sum_R)^{-1}$ is the retarded Green's function, where $H$ is the Hamiltonian and $S$ is the overlap matrix (both of them obtained from SIESTA). Finally the room temperature electrical conductance was computed from the formula

$G = G_0 \int_{-\infty}^{\infty} dE\, T(E)(-\frac{df(E)}{dE})$ where $f(\mathrm{E}) = [e^{\beta(E-E_F)} + 1]^{-1}$ is the Fermi function, $\beta = 1/k_BT$, $E_F$ is the Fermi energy and $G_0 = \left(\frac{2e^2}{h}\right)$ is the quantum of conductance. Since the quantity $(-\frac{df(E)}{dE})$ is a probability distribution peaked at $E=E_F$, with a width of order $k_BT$, the above expression shows that $G/G_0$ is obtained by averaging $T(E)$ over an energy range of order $k_BT$ in the vicinity of $E=E_F$. It is well-known that the Fermi energy $E_F^{DFT}$ predicted by DFT is not usually reliable and therefore Figures 7 and 8 show plots of $G/G_0$ as a function of $E_F$ - $E_F^{DFT}$. To determine $E_F$, we compared the predicted values of all molecules with the experimental values and chose a single common value of $E_F$ which gave the closest overall agreement. This yielded a value of $E_F$ - $E_F^{DFT}$ = –0.14 eV, which is used in all theoretical results.

**AUTHOR INFORMATION** The authors declare no competing financial interest.

**ASSOCIATED CONTENT** Experimental details; Tables of electrochemical data and plots of voltammograms; Further discussion of electrochemical and spectroelectrochemical results with plots of UV-vis-NIR and IR spectra; Details of deposition of [**2-Fe**](PF)$_6$ on Au surfaces and characterisation; Further text describing the role of the electrolyte on the electrical response of the junction; Details of the single molecule conductance experiments and plots of conductance traces from the $I(s)$ experiments. The Supporting Information is available free of charge on the ACS Publications website at DOI….

**ACKNOWLEDGEMENTS**

Mr Daniel Cripps (University of Reading) is thanked for his valuable contribution to this work, in particular the CV and SERS measurements of complexes deposited on the gold electrode surface. D.C.M., R.J.D., F.H., S.J.H., R.J.N., C.J.L. and P.J.L. thank EPSRC for funding (EPSRC grants EP/K007785/1, EP/H035184/1, EP/K007548/1, EP/K00753X/1, EP/N017188/1, EP/M014452/1). F.H. also gratefully acknowledges the University of Reading for the support of the Reading Spectroelectrochemistry center (University Project D14-015 Spectroelectrochemical Cells). P.J.L. holds an ARC Future Fellowship (FT120100073) and gratefully acknowledges funding for this work from the ARC (DP140100855). C.J.L. and O.A.A. acknowledge financial support from the Ministry of Higher Education and Scientific Research of Iraq. C. J. L. acknowledges funding from the EU through the FP7 ITN MOLESCO (project number 212942).

**REFERENCES**

(1) Nichols, R. J.; Haiss, W.; Higgins, S. J.; Leary, E.; Martin, S.; Bethell, D. *Phys. Chem. Chem. Phys.* **2010**, *12*, 2801.

(2) Florian, S.; Emanuel, L. *J. Phys. Condens. Matter* **2014**, *26*, 474201.

(3) Sun, L.; Diaz-Fernandez, Y. A.; Gschneidtner, T. A.; Westerlund, F.; Lara-Avila, S.; Moth-Poulsen, K. *Chem. Soc. Rev.* **2014**, *43*, 7378.

(4) Bergfield, J. P.; Ratner, M. A. *Phys. Status Solidi (b)* **2013**, *250*, 2249.

(5) Son, J. Y.; Song, H. *Curr. App. Phys.* **2013**, *13*, 1157.

(6) Lu, W.; Lieber, C. M. *Nat Mater* **2007**, *6*, 841.

(7) Liu, H.; Wang, N.; Zhao, J.; Guo, Y.; Yin, X.; Boey, F. Y. C.; Zhang, H. *ChemPhysChem* **2008**, *9*, 1416.

(8) Kaliginedi, V.; Moreno-García, P.; Valkenier, H.; Hong, W.; García-Suárez, V. M.; Buiter, P.; Otten, J. L. H.; Hummelen, J. C.; Lambert, C. J.; Wandlowski, T. *J. Am. Chem. Soc.* **2012**, *134*, 5262.

(9) Wang, C.; Batsanov, A. S.; Bryce, M. R.; Martín, S.; Nichols, R. J.; Higgins, S. J.; García-Suárez, V. M.; Lambert, C. J. *J. Am. Chem. Soc.* **2009**, *131*, 15647.

(10) Ashwell, G.; Urasinska, B.; Wang, C.; Bryce, M.; Grace, I.; Lambert, C. *Chemical Communications* **2006**, 4706.

(11) Zeng, X.; Wang, C.; Bryce, M.; Batsanov, A.; Sirichantaropass, S.; Garcia-Suarez, V.; Lambert, C.; Sage, I. *European Journal of Organic Chemistry* **2007**, 5244.

(12) Wang, C.; Bryce, M.; Gigon, J.; Ashwell, G.; Grace, I.; Lambert, C. *Journal of Organic Chemistry* **2008**, *73*, 4810.

(13) Higgins, S. J.; Nichols, R. J.; Martin, S.; Cea, P.; van der Zant, H. S. J.; Richter, M. M.; Low, P. J. *Organometallics* **2011**, *30*, 7.

(14) Georgiev, V. P.; Mohan, P. J.; DeBrincat, D.; McGrady, J. E. *Coord. Chem. Rev.* **2013**, *257*, 290.

(15) Cummings, S. P.; Savchenko, J.; Ren, T. *Coord. Chem. Rev.* **2011**, *255*, 1587.

(16) Natelson, D.; Yu, L. H.; Ciszek, J. W.; Keane, Z. K.; Tour, J. M. *Chem. Phys.* **2006**, *324*, 267.

(17) Natelson, D.; Yu, L. H.; Keane, Z. K.; Ciszek, J. W.; Tour, J. M. *Physica B: Condens. Matter* **2008**, *403*, 1526.

(18) Kikoin, K.; Kiselev, M. N.; Wegewijs, M. R. *Phys. Rev. Lett.* **2006**, *96*, 176801.

(19) Rigaut, S. *Dalton Trans.* **2013**, *42*, 15859.

(20) Low, P. J. *Dalton Trans.* **2005**, 2821.

(21) Sedghi, G.; Sawada, K.; Esdaile, L. J.; Hoffmann, M.; Anderson, H. L.; Bethell, D.; Haiss, W.; Higgins, S. J.; Nichols, R. J. *J. Am. Chem. Soc.* **2008**, *130*, 8582.

(22) Jurow, M.; Schuckman, A. E.; Batteas, J. D.; Drain, C. M. *Coord. Chem. Rev.* **2010**, *254*, 2297.

(23) Wen, H.-M.; Yang, Y.; Zhou, X.-S.; Liu, J.-Y.; Zhang, D.-B.; Chen, Z.-B.; Wang, J.-Y.; Chen, Z.-N.; Tian, Z.-Q. *Chem. Sci.* **2013**, *4*, 2471.

(24) Lissel, F.; Schwarz, F.; Blacque, O.; Riel, H.; Lörtscher, E.; Venkatesan, K.; Berke, H. *J. Am. Chem. Soc.* **2014**, *136*, 14560.

(25) Schwarz, F.; Kastlunger, G.; Lissel, F.; Riel, H.; Venkatesan, K.; Berke, H.; Stadler, R.; Lörtscher, E. *Nano Lett.* **2014**, *14*, 5932.

(26) Meng, F.; Hervault, Y.-M.; Shao, Q.; Hu, B.; Norel, L.; Rigaut, S.; Chen, X. *Nat. Commun.* **2014**, *5*, 3023.

(27) Meng, F.; Hervault, Y.-M.; Norel, L.; Costuas, K.; Van Dyck, C.; Geskin, V.; Cornil, J.; Hng, H. H.; Rigaut, S.; Chen, X. *Chem. Sci.* **2012**, *3*, 3113.

(28) Marques-Gonzalez, S.; Yufit, D. S.; Howard, J. A. K.; Martin, S.; Osorio, H. M.; Garcia-Suarez, V. M.; Nichols, R. J.; Higgins, S. J.; Cea, P.; Low, P. J. *Dalton Trans.* **2013**, *42*, 338.

(29) Ng, Z.; Loh, K. P.; Li, L.; Ho, P.; Bai, P.; Yip, J. H. K. *ACS Nano* **2009**, *3*, 2103.

(30) Haga, M.; Takasugi, T.; Tomie, A.; Ishizuya, M.; Yamada, T.; Hossain, M. D.; Inoue, M. *Dalton Trans.* **2003**, 2069.

(31) Yang, W.; Zhong, Y.; Yoshikawa, S.; Shao, J.; Masaoka, S.; Sakai, K.; Yao, J.; Haga, M. *Inorg. Chem.* **2012**, *51*, 890.

(32) Gupta, T.; Mondal, P. C.; Kumar, A.; Jeyachandran, Y. L.; Zharnikov, M. *Adv. Funct. Mater.* **2013**, *23*, 4227.

(33) Musumeci, C.; Zappalà, G.; Martsinovich, N.; Orgiu, E.; Schuster, S.; Quici, S.; Zharnikov, M.; Troisi, A.; Licciardello, A.; Samorì, P. *Adv. Mater.* **2014**, *26*, 1688.

(34) Traulsen, C. H. H.; Darlatt, E.; Richter, S.; Poppenberg, J.; Hoof, S.; Unger, W. E. S.; Schalley, C. A. *Langmuir* **2012**, *28*, 10755.

(35) Welte, L.; Calzolari, A.; Di Felice, R.; Zamora, F.; Gomez-Herrero, J. *Nat Nano* **2010**, *5*, 110.

(36) Nishimori, Y.; Kanaizuka, K.; Kurita, T.; Nagatsu, T.; Segawa, Y.; Toshimitsu, F.; Muratsugu, S.; Utsuno, M.; Kume, S.; Murata, M.; Nishihara, H. *Chem. Asian J.* **2009**, *4*, 1361.

(37) Sakamoto, R.; Katagiri, S.; Maeda, H.; Nishihara, H. *Coord. Chem. Rev.* **2013**, *257*, 1493.

(38) Maeda, H.; Sakamoto, R.; Nishihara, H. *Polymer* **2013**, *54*, 4383.

(39) Ruben, M.; Landa, A.; Loertscher, E.; Riel, H.; Mayor, M.; Goerls, H.; Weber, H. B.; Arnold, A.; Evers, F. *Small* **2008**, *4*, 2229.

(40) Inatomi, J.; Fujii, S.; Marqués-González, S.; Masai, H.; Tsuji, Y.; Terao, J.; Kiguchi, M. *J Phys. Chem. C* **2015**, *119*, 19452.

(41) Ponce, J.; Arroyo, C. R.; Tatay, S.; Frisenda, R.; Gavina, P.; Aravena, D.; Ruiz, E.; van der Zant, H. S. J.; Coronado, E. *J. Am. Chem. Soc.* **2014**, *136*, 8314.

(42) Albrecht, T.; Guckian, A.; Kuznetsov, A. M.; Vos, J. G.; Ulstrup, J. *J. Am. Chem. Soc.* **2006**, *128*, 17132.

(43) Albrecht, T.; Moth-Poulsen, K.; Christensen, J. B.; Hjelm, J.; Bjørnholm, T.; Ulstrup, J. *J. Am. Chem. Soc.* **2006**, *128*, 6574.

(44) Kastlunger, G.; Stadler, R. *Phys. Rev. B* **2013**, *88*, 035418.

(45) Albrecht, T.; Guckian, A.; Ulstrup, J.; Vos, J. G. *Nano Lett.* **2005**, *5*, 1451.

(46) Osorio, E. A.; Moth-Poulsen, K.; van der Zant, H. S. J.; Paaske, J.; Hedegård, P.; Flensberg, K.; Bendix, J.; Bjørnholm, T. *Nano Lett.* **2010**, *10*, 105.

(47) Park, T.; Sidorov, V. A.; Ronning, F.; Zhu, J. X.; Tokiwa, Y.; Lee, H.; Bauer, E. D.; Movshovich, R.; Sarrao, J. L.; Thompson, J. D. *Nature* **2008**, *456*, 366.

(48) Nakamura, H.; Ohto, T.; Ishida, T.; Asai, Y. *J. Am. Chem. Soc.* **2013**, *135*, 16545.

(49) Chen, I. W. P.; Fu, M.-D.; Tseng, W.-H.; Yu, J.-Y.; Wu, S.-H.; Ku, C.-J.; Chen, C.-h.; Peng, S.-M. *Angew. Chem. Int. Ed.* **2006**, *45*, 5814.

(50) DeBrincat, D.; Keers, O.; McGrady, J. E. *Chem. Comm.* **2013**, *49*, 9116.

(51) Park, J.; Pasupathy, A. N.; Goldsmith, J. I.; Chang, C.; Yaish, Y.; Petta, J. R.; Rinkoski, M.; Sethna, J. P.; Abruna, H. D.; McEuen, P. L.; Ralph, D. C. *Nature* **2002**, *417*, 722.

(52) Liang, W.; Shores, M. P.; Bockrath, M.; Long, J. R.; Park, H. *Nature* **2002**, *417*, 725.

(53) Parks, J. J.; Champagne, A. R.; Costi, T. A.; Shum, W. W.; Pasupathy, A. N.; Neuscamman, E.; Flores-Torres, S.; Cornaglia, P. S.; Aligia, A. A.; Balseiro, C. A.; Chan, G. K.-L.; Abruña, H. D.; Ralph, D. C. *Science* **2010**, *328*, 1370.

(54) Herrmann, C.; Solomon, G. C.; Ratner, M. A. *J. Phys. Chem. C* **2010**, *114*, 20813.

(55) Jia, C.; Guo, X. *Chem. Soc. Rev.* **2013**, *42*, 5642.

(56) Leary, E.; La Rosa, A.; Gonzalez, M. T.; Rubio-Bollinger, G.; Agrait, N.; Martin, N. *Chem. Soc. Rev.* **2015**, *44*, 920.

(57) Whetten, R. L.; Price, R. C. *Science* **2007**, *318*, 407.

(58) Lee, S. U.; Mizuseki, H.; Kawazoe, Y. *Phys. Chem. Chem. Phys.* **2010**, *12*, 11763.

(59) Hakkinen, H. *Nat Chem* **2012**, *4*, 443.

(60) Schönherr, H.; Kremer, F. J. B.; Kumar, S.; Rego, J. A.; Wolf, H.; Ringsdorf, H.; Jaschke, M.; Butt, H. J.; Bamberg, E. *J. Am. Chem. Soc.* **1996**, *118*, 13051.

(61) Capozzi, B.; Dell, E. J.; Berkelbach, T. C.; Reichman, D. R.; Venkataraman, L.; Campos, L. M. *J. Am. Chem. Soc.* **2014**, *136*, 10486.

(62) Dell, E. J.; Capozzi, B.; Xia, J. L.; Venkataraman, L.; Campos, L. M. *Nat. Chem.* **2015**, *7*, 209.

(63) Su, T. A.; Li, H. X.; Steigerwald, M. L.; Venkataraman, L.; Nuckolls, C. *Nat. Chem.* **2015**, *7*, 215.

(64) Yoshida, K.; Pobelov, I. V.; Manrique, D. Z.; Pope, T.; Mészáros, G.; Gulcur, M.; Bryce, M. R.; Lambert, C. J.; Wandlowski, T. *Sci. Rep.* **2015**, *5*, 9002.

(65) Gulcur, M.; Moreno-García, P.; Zhao, X.; Baghernejad, M.; Batsanov, A. S.; Hong, W.; Bryce, M. R.; Wandlowski, T. *Chem. – Eur. J.* **2014**, *20*, 4653.

(66) Frisenda, R.; Tarkuc, S.; Galan, E.; Perrin, M. L.; Eelkema, R.; Grozema, F. C.; van der Zant, H. S. J. *Beilstein J. Nanotechnol.* **2015**, *6*, 1558.

(67) Endou, M.; Ie, Y.; Kaneda, T.; Aso, Y. *J. Org. Chem.* **2007**, *72*, 2659.

(68) Pera, G.; Martín, S.; Ballesteros, L. M.; Hope, A. J.; Low, P. J.; Nichols, R. J.; Cea, P. *Chem. – Eur. J.* **2010**, *16*, 13398.

(69) Martín, S.; Pera, G.; Ballesteros, L. M.; Hope, A. J.; Marqués-González, S.; Low, P. J.; Pérez-Murano, F.; Nichols, R. J.; Cea, P. *Chem. – Eur. J.* **2014**, *20*, 3421.

(70) Petrov, E. G.; Marchenko, A.; Kapitanchuk, O. L.; Katsonis, N.; Fichou, D. *Mol. Cryst. Liq. Cryst.* **2014**, *589*, 3.

(71) Marchenko, A.; Katsonis, N.; Fichou, D.; Aubert, C.; Malacria, M. *J. Am. Chem. Soc.* **2002**, *124*, 9998.

(72) Katsonis, N.; Marchenko, A.; Taillemite, S.; Fichou, D.; Chouraqui, G.; Aubert, C.; Malacria, M. *Chem. – Eur. J.* **2003**, *9*, 2574.

(73) Katsonis, N.; Marchenko, A.; Fichou, D.; Barrett, N. *Surf. Sci.* **2008**, *602*, 9.

(74) Nion, A.; Katsonis, N.; Marchenko, A.; Aubert, C.; Fichou, D. *New J. Chem.* **2013**, *37*, 2261.

(75) Grosshenny, V.; Romero, F. M.; Ziessel, R. *J. Org. Chem.* **1997**, *62*, 1491.

(76) Constable, E. C.; Housecroft, C. E.; Medlycott, E.; Neuburger, M.; Reinders, F.; Reymann, S.; Schaffner, S. *Inorg. Chem. Comm.* **2008**, *11*, 518.

(77) England, J.; Scarborough, C. C.; Weyhermüller, T.; Sproules, S.; Wieghardt, K. *Eur. J. Inorg. Chem.* **2012**, *2012*, 4605.

(78) Ballesteros, L. M.; Martin, S.; Cortes, J.; Marques-Gonzalez, S.; Perez-Murano, F.; Nichols, R. J.; Low, P. J.; Cea, P. *Adv. Mater. Inter.* **2014**, *1*, 1400128.

(79) Kamenetska, M.; Quek, S. Y.; Whalley, A. C.; Steigerwald, M. L.; Choi, H. J.; Louie, S. G.; Nuckolls, C.; Hybertsen, M. S.; Neaton, J. B.; Venkataraman, L. *J. Am. Chem. Soc.* **2010**, *132*, 6817.

(80) Tuccitto, N.; Ferri, V.; Cavazzini, M.; Quici, S.; Zhavnerko, G.; Licciardello, A.; Rampi, M. A. *Nat Mater* **2009**, *8*, 41.

(81) Wang, L.-J.; Yong, A.; Zhou, K.-G.; Tan, L.; Ye, J.; Wu, G.-P.; Xu, Z.-G.; Zhang, H.-L. *Chem. Asian J.* **2013**, *8*, 1901.

(82) Venkataraman, L.; Klare, J. E.; Nuckolls, C.; Hybertsen, M. S.; Steigerwald, M. L. *Nature* **2006**, *442*, 904.

(83) Katsonis, N.; Marchenko, A.; Fichou, D.; Barrett, N. *Surf. Sci.* **2008**, *602*, 9.

(84) Hakkinen, H. *Nat. Chem.* **2012**, *4*, 443.

(85) Sladek, A.; Schmidbaur, H. *Z. Naturforsch., B: Chem. Sci.* **1996**, *51*, 1207.

(86) Akermark, B.; Vitagliano, A. *Organometallics* **1985**, *4*, 1275.

(87) Haiss, W.; Lackey, D.; Sass, J. K.; Besocke, K. H. *J. Chem. Phys.* **1991**, *95*, 2193.

(88) Haiss, W.; van Zalinge, H.; Higgins, S. J.; Bethell, D.; Höbenreich, H.; Schiffrin, D. J.; Nichols, R. J. *J. Am. Chem. Soc.* **2003**, *125*, 15294.

(89) Krejcik, M.; Danek, M.; Hartl, F. *J. Electroanal. Chem.* **1991**, *317*, 179.

(90) Perdew, J. P.; Burke, K.; Ernzerhof, M. *Phys. Rev. Lett.* **1996**, *77*, 3865.

(91) Soler, J. M.; Artacho, E.; Gale, J. D.; Garcia, A.; Junquera, J.; Ordejon, P.; Sanchez-Portal, D. *J. Phys. Condes. Matter* **2002**, *14*, 2745.

(92) Ferrer, J.; Lambert, C. J.; Garcia-Suarez, V. M.; Manrique, D. Z.; Visontai, D.; Oroszlany, L.; Rodriguez-Ferradas, R.; Grace, I.; Bailey, S. W. D.; Gillemot, K.; Sadeghi, H.; Algharagholy, L. A. *New J. Phys.* **2014**, *16*.

Table of Contents Entry

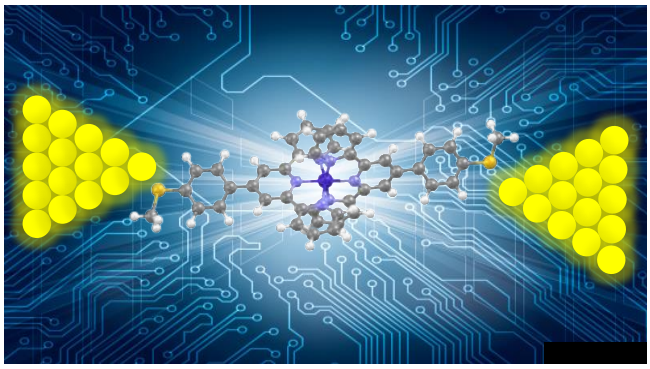

TOC Synopsis

The bis-2,2′:6′,2″-terpyridine complexes featuring Ru(II), Fe(II) and Co(II) metal ions and trimethylsilylethynyl ($Me_3SiC{\equiv}C$-) or thiomethyl (SMe) surface contact groups behave as tunneling barriers in single molecule junctions, with conductance properties determined more by the strength of the electrode-molecule contact and the structure of the ‘linker’ than the nature of the metal or redox properties of the complex.